



6G Digital Twin Enabled Channel Modeling for Beijing Central Business District

LU Mengyuan^{1,2}, BAI Lu^{1,3,4}, HAN Zengrui⁵,
HUANG Ziwei⁵, LU Shiliang^{1,2}, CHENG Xiang⁵

(1. Joint SDU-NTU Centre for Artificial Intelligence Research (C-FAIR), Shandong University, Jinan 250101, China;
2. School of Software, Shandong University, Jinan 250101, China;
3. National Mobile Communications Research Laboratory, Southeast University, Nanjing 214135, China;
4. Shandong Research Institute of Industrial Technology, Jinan 250100, China;
5. School of Electronics, Peking University, Beijing 100871, China)

DOI: 10.12142/ZTECOM.202502005

<https://kns.cnki.net/kcms/detail/34.1294.TN.20250521.0912.002.html>,
published online May 21, 2025

Manuscript received: 2025-01-20

Abstract: A novel digital twin (DT) enabled channel model for 6G vehicular communications in Beijing Central Business District (Beijing CBD) is proposed, which can support the design of intelligent transportation systems (ITSs). A DT space for Beijing CBD is constructed, and two typical transportation periods, i.e., peak and off-peak hours, are considered to characterize the vehicular communication channel better. Based on the constructed DT space, a DT-enabled vehicular communication dataset is developed, including light detection and ranging (LiDAR) point clouds, RGB images, and channel information. With the assistance of LiDAR point clouds and RGB images, the scatterer parameters, including number, distance, angle, power, and velocity, are analyzed under different transportation periods. The channel non-stationarity and consistency are mimicked in the proposed model. The key channel statistical properties are derived and simulated. Compared to ray-tracing (RT) results, the accuracy of the proposed model is verified.

Keywords: DT; channel modeling; 6G vehicular communications; Beijing CBD; DT-enabled vehicular communication dataset

Citation (Format 1): LU M Y, BAI L, HAN Z R, et al. 6G digital twin enabled channel modeling for Beijing central business district [J]. *ZTE Communications*, 2025, 23(2): 31 - 45. DOI: 10.12142/ZTECOM.202502005

Citation (Format 2): M. Y. Lu, L. Bai, Z. R. Han, et al., "6G digital twin enabled channel modeling for Beijing central business district," *ZTE Communications*, vol. 23, no. 2, pp. 31 - 45, Jun. 2025. doi: 10.12142/ZTECOM.202502005.

1 Introduction

With the development of 6G wireless networks, the demands for high-performance communications are increasing, particularly in densely populated and built-up areas such as central business districts (CBDs). As the core business hub of China's capital, Beijing CBD faces exceptionally high wireless communication demands. The unique architecture and dense traffic flow

in this area have a significant impact on wireless channel characteristics. 6G networks are expected to meet these challenges by providing wider coverage, higher data rates, and lower latency. Intelligent transportation systems (ITSs), as a key technology to enhance traffic management and transportation efficiency, promote traffic safety and efficiency through the application of information technology, communication equipment, computing technology, and artificial intelligence (AI). Vehicular communication is an important part of ITS, which significantly improves road safety via real-time communications between vehicles^[1]. However, in high-density and high-traffic urban environments like Beijing CBD, vehicular communications are challenged by complex and dynamic wireless channel conditions. Accurate channel modeling is essential to ensure the reliability and efficiency of vehicular communications. Furthermore, traffic density differs significantly between peak and off-peak hours. As a result, more accurate channel models are essentially required to depict the wireless communication environment and to

This work was supported in part by the National Natural Science Foundation of China under Grant Nos. 62371273, 62125101 and 62341101; the Taishan Scholars Program under Grant No. tsqn202312307; the Young Elite Scientists Sponsorship Program by CAST under Grant No. YESS20230372; the Shandong Natural Science Foundation under Grant No. ZR2023YQ058; the New Cornerstone Science Foundation through the Xplorer Prize; the Xiaomi Young Talents Program; the open research fund of National Mobile Communications Research Laboratory, Southeast University under Grant No. 2025D04; the China National Postdoctoral Program for Innovative Talents under Grant No. BX20240007; the China Postdoctoral Science Foundation under Grant No. 2024M760111; the Beijing Natural Science Foundation under Grant No. 4254067.

guide a more precise design of the communication system.

Digital twin (DT) is a digital reconstruction of physical entities and can be utilized as an efficient method to characterize, simulate, and visualize physical entities^[2]. DT has advantages in representing physical entities that are difficult to model and replicate. DT enables the creation of a virtual replica of the real-world environment, which allows the dynamics of the channel to be accurately modeled.

Recent studies have integrated DT with wireless communication systems. DT is utilized to construct virtual models that simulate the real world and facilitate data acquisition based on the constructed models. A platform for DT was proposed in Ref. [3], along with a synthetic dataset combining the data obtained through the real world and those obtained through virtual copies. This approach reduces the burden of collecting real-world channel data and significantly decreases the system overhead. DT can also reduce the data acquisition overhead of the communication system and improve the system accuracy. In Ref. [4], the authors introduced a ray-tracing (RT) oriented approach for DT demonstration of radio propagation in multiple frequency bands from microwave to visible light. Furthermore, a super-resolution modeling method was developed by fusing RT and AI algorithms to improve the stability and accuracy of communications. The authors in Ref. [5] utilized site-specific DT models to train deep learning (DL) models. The proposed DT-based method generates site-specific synthetic channel state information (CSI) data through 3D modeling and RT methods, enabling effective training of DL models while reducing the overhead of real-world data collection. To further improve model performance, an online data selection approach is used to refine the DL model training with a small real-world CSI dataset. Since DT can contribute to balancing the overhead and the accuracy of communication systems, it has been widely adopted in various communication scenarios, such as UAV and vehicular communication systems. A framework for DT-based UAV applications was proposed in Ref. [6], where a task manager orchestrated interactions between the DT system and physical UAVs. DT can assist UAVs to achieve more efficient flight paths and reduce energy consumption, which improves the efficiency of UAV communication systems. For vehicular communication systems, a city-model-aware DL algorithm for dynamic channel estimation in urban vehicular environments was proposed in Ref. [7]. The proposed model gained a balance between accuracy and timeliness. In summary, DT effectively reduces the overhead of data acquisition and significantly improves system accuracy by reflecting the dynamic changes of the environment in real time. DTs have been applied to a variety of typical communication scenarios. However, accurate comprehension and modeling of the environment are essential to further enhance system security and reliability.

To accurately depict the communication environment, the

channel characteristics between the transmitter (TX) and the receiver (RX) need to be precisely characterized. Therefore, channel modeling is the cornerstone of communication systems, and more accurate channel models are essential to further improve the efficiency of communication systems. Conventional channel modeling approaches, including stochastic and deterministic models, have significantly contributed to wireless communication systems. However, the methods have limitations when applied to complex and dynamic urban environments. For example, stochastic models depend on predefined assumptions, which may not accurately capture variations in specific scenarios^[8]. Deterministic models, such as RT methods, provide better accuracy with high computational overhead and the difficulty of real-time adjustment^[9].

DT provides a new paradigm for channel modeling as it enables accurate physical-virtual world mapping. By precisely modeling and dynamically updating the virtual environment, DT can capture the changing characteristics in the environment in real time. When integrated with machine learning (ML) algorithms, DT can also extract key characteristics from complex scenarios and realize high-precision modeling of diverse channel characteristics. In Ref. [10], the authors proposed a channel modeling approach based on generative adversarial networks for DT environments, which can generate channel data with a statistical distribution that closely matches the measured channel. A data-driven continuous trajectory modeling method for a user equipment with a DT channel was proposed in Ref. [11]. This method generates channel models whose spatial and temporal characteristics match the real-world wireless channels. Nevertheless, current studies on DT-based channel modeling are still at the preliminary stage, particularly on high-precision modeling in dynamic environments. Most existing DT-based channel models cannot handle high-mobility vehicular communication scenarios. Therefore, there is an urgent need to explore DT-based methods for improving the accuracy of vehicular communication channel modeling.

To fill this gap, we explore the application of DT to channel modeling and select a typical urban communication scenario, i. e., vehicular communications within Beijing CBD. We propose a new method of channel modeling based on DT for complex urban environments. The main contributions and novelties of this paper are summarized as follows.

- 1) A new reliable DT space for Beijing CBD is constructed, where the physical and electromagnetic spaces are precisely aligned by AirSim and Wireless InSite. It provides a highly accurate virtual environment for channel modeling.

- 2) A DT-based dataset is constructed for Beijing CBD for the first time, which includes sensory data, i. e., light detection and ranging (LiDAR) point clouds, RGB images, and channel data. The dataset is constructed in complex and dynamic scenarios and comprehensively captures the unique characteristics of vehicular communications in ur-

ban environments.

3) A DT-enabled vehicular communication channel model for Beijing CBD is developed, which models and analyzes the channel characteristics of peak and off-peak hours in Beijing CBD for the first time. Furthermore, the channel parameters, e.g., number, distance, angle, and power of scatterers with different velocities, are developed under different transportation periods.

4) Based on the proposed channel model for Beijing CBD, key channel statistical properties, i.e., time-frequency correlation function (TF-CF) and Doppler power spectral density (DPSD), are derived and simulated. According to the simulation results, the effect of different transportation periods on the channel statistical properties is investigated. Simulation results are consistent with the experimental results based on RT, which verifies the accuracy and practicability of the channel model based on DT.

The remainder of this paper is organized as follows. Section 2 describes the DT space for Beijing CBD. Section 3 proposes a novel DT-enabled vehicular communication channel model for Beijing CBD. Section 4 presents the statistical properties of the vehicular communication channel and compares the simulation results with those based on RT. Finally, Section 5 concludes the paper.

2 DT Space for Beijing CBD

Beijing CBD provides a unique scenario for ITS applications with its high-density buildings, complex transportation networks, and diverse communication requirements. However, conventional channel modeling methods face several challenges in complex urban scenarios, particularly in modeling multipath propagation and dynamic changes. DT technology enables the construction of digital spaces that match the real world to accurately reflect real-time environmental changes. Therefore, a DT space for Beijing CBD is constructed to achieve accurate modeling of the physical environment and dynamic traffic characteristics of the area. This DT space provides a robust platform for channel modeling, which can support the research of high-precision vehicular communication systems.

2.1 Construction of DT Space for Beijing CBD

In Beijing CBD, the diversity of building distribution and types has a significant impact on the signal propagation characteristics. The CBD, as the core business district of the capital, features high building density with numerous high-rise and modern office buildings. The different heights, shapes, layouts, and building materials of these buildings significantly influence wireless signal propagation. As for transportation, the traffic volume in Beijing CBD peaks during rush hours, and vehicle quantity and density directly affect wireless signal transmission.

To construct a DT space that can match the real environ-

ment well, we first use Blender, a 3D modeling tool, to establish a scenario identical to Beijing CBD, leveraging satellite maps and 3D models of the buildings. To ensure the accuracy of the constructed scenario, the heights, sizes, and inter-building distances are strictly consistent with the real world. Then we utilize Wireless InSite in Ref. [12] to build the electromagnetic space. The process involves importing the constructed 3D model into Wireless InSite. Then the propagation parameters are set with a frequency of 5.9 GHz, a bandwidth of 20 MHz, and an omnidirectional antenna for transceivers. Parameters related to electromagnetic phenomena, such as reflections and dispersions, are configured in Wireless InSite to simulate channel characteristics in specific frequency bands. Meanwhile, the influence of buildings, vehicles, and other obstacles in radio propagation is ensured to be effectively reflected. Two scenarios are constructed for investigating the effect of peak and off-peak traffic conditions on channel characteristics. The objects in the two scenarios remain identical except for the number of vehicles. Vehicles are 57 during peak hours and 34 during off-peak hours. After establishing the electromagnetic environment model, the model exported from Wireless InSite is imported into the AirSim platform for detailed visualization, which provides a simulation of the visual and dynamic environment similar to Ref. [13]. Each vehicle in AirSim is equipped with sensory devices, i.e., RGB cameras and LiDAR devices. The dynamic vehicular trajectories simulated in AirSim remains identical to those in Wireless InSite. With the precisely aligned scenarios in Wireless InSite and AirSim, the real-world physical environment is accurately replicated in the virtual space. The environment consistency across different platforms is maintained and dynamically updated, facilitating the construction of a highly reproducible DT space.

2.2 Data Collection and Processing in DT Space

Beijing CBD scenarios in Wireless InSite and AirSim are presented in Fig. 1. To construct the DT-based Beijing CBD vehicular communication dataset, a simulation setup in Wireless InSite and AirSim is required. The number of simulation snapshots is set to 300 with a time interval of 0.01 s. The batch generation of the scenarios is set up through MATLAB scripts in Wireless InSite, and the position of the vehicles is simulated through Python scripts set up by frame in AirSim. The vehicular trajectories during off-peak hours are shown in Fig. 2. Sensory data (LiDAR point clouds and RGB images) and communication data are collected. Simultaneously, the moving vehicles establish the Beijing CBD vehicle communication dataset based on DT. The communication links simulated in both transportation periods are identical, as shown in Fig. 2. The constructed dataset consists of 10 800 LiDAR point clouds, 10 800 RGB images, and 9 000 communication link data.

The high mobility of multiple transceivers and scatterers

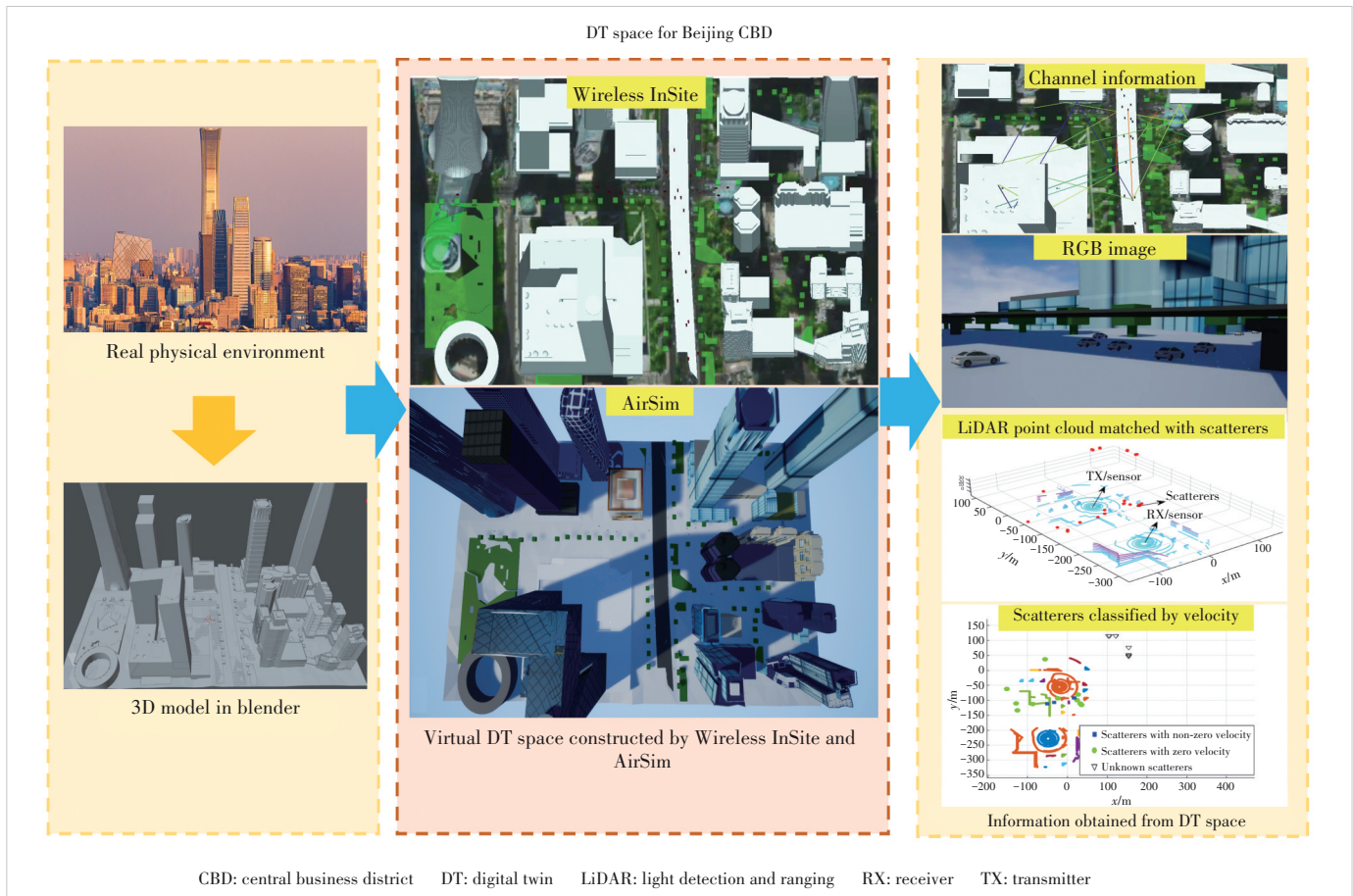


Figure 1. DT space for Beijing CBD vehicular communication scenarios

results in complex characterization. Therefore, the detection of the velocity properties of scatterers is extremely significant. With the support of sensing data (LiDAR point clouds and RGB data), zero velocity scatterers (ZVSes) and non-zero velocity scatterers (NVSES) can be detected and matched to static objects and dynamic vehicles. The LiDAR point clouds, combined with the clustering algorithm and RGB images, can effectively distinguish between the ZVS and those with non-zero velocity. The point cloud data are pre-processed and then clustered using the density-based spatial clustering of applications with noise (DBSCAN) clustering algorithm in Ref. [14], a typical ML algorithm for grouping the point clouds. ZVS sets usually correspond to static objects such as buildings, which remain stable over multiple time frames, while NVS sets correspond to dynamic objects (vehicles), whose positions change over time. The two types of scatterers can be accurately distinguished by matching point cloud clusters in different time frames and combining them with velocity estimation methods. Some scatterers cannot correspond to any object due to exceeding the detection range of the LiDAR sensor. Since unknown scatterers are usually far away from the transceiver and the received power via them is

very small, they can be ignored in the channel realization. Fig. 1 characterizes the scatterers extracted from the RT-based wireless channel data.

3 DT Enabled Channel Modeling

Based on the constructed DT space, a DT-enabled vehicular communication channel model for the Beijing CBD area is proposed, which considers the impact of different traffic densities for peak and off-peak hour periods. Moreover, to parameterize the proposed model more accurately, the scatterer properties, i.e., number, distance, angle, and power of scatterers with different velocities, are modeled and analyzed. Furthermore, the channel non-stationarity and consistency in the time domains are studied.

3.1 Framework of DT-Enabled Channel Model for Beijing CBD

The channel impulse response (CIR) of the vehicular communication channel $h(t, \tau)$, i.e., the CIR of the transmission link from the i -th vehicle to the j -th vehicle, can be represented as:



Figure 2. Vehicular trajectories and communication links under off-peak DT-enabled Beijing CBD scenarios

$$\begin{aligned}
 h(t, \tau) = & \underbrace{\sqrt{\frac{\Omega(t)}{\Omega(t) + 1}} h^{\text{LoS}}(t) \delta(\tau - \tau^{\text{LoS}}(t))}_{\text{LoS}} + \\
 & \underbrace{\sqrt{\frac{\eta^{\text{GR}}(t)}{\Omega(t) + 1}} h^{\text{GR}}(t) \delta(\tau - \tau^{\text{GR}}(t))}_{\text{Ground Reflection}} + \\
 & \sum_{p=1}^{N_z^z(t)} \sum_{n_p=1}^{N_z^z(t)} \sqrt{\frac{\eta^z(t)}{\Omega(t) + 1}} h_{p,n_p}^z(t) \delta(\tau - \tau_{p,n_p}^z(t)) + \\
 & \underbrace{\sum_{q=1}^{N^{nz}(t)} \sum_{n_q=1}^{N^{nz}(t)} \sqrt{\frac{\eta^{nz}(t)}{\Omega(t) + 1}} h_{q,n_q}^{nz}(t) \delta(\tau - \tau_{q,n_q}^{nz}(t))}_{\text{NLoS}} \quad (1),
 \end{aligned}$$

where $\Omega(t)$ represents the Ricean factor of the transmission link from the i -th vehicle to the j -th vehicle. $\eta^{\text{GR}}(t)$, $\eta^z(t)$, and $\eta^{nz}(t)$ are the power ratios of the ground reflection component, component via clusters with zero velocity, and component via clusters with non-zero velocity in the transmission link from the i -th vehicle to the j -th vehicle; they satisfy $\eta^{\text{GR}}(t) +$

$\eta^z(t) + \eta^{nz}(t) = 1$. The representation of the proposed DT-enabled vehicular communication channel model for Beijing CBD is depicted in Fig. 3. The distance between transceivers is $D_{i,j}(t_0)$.

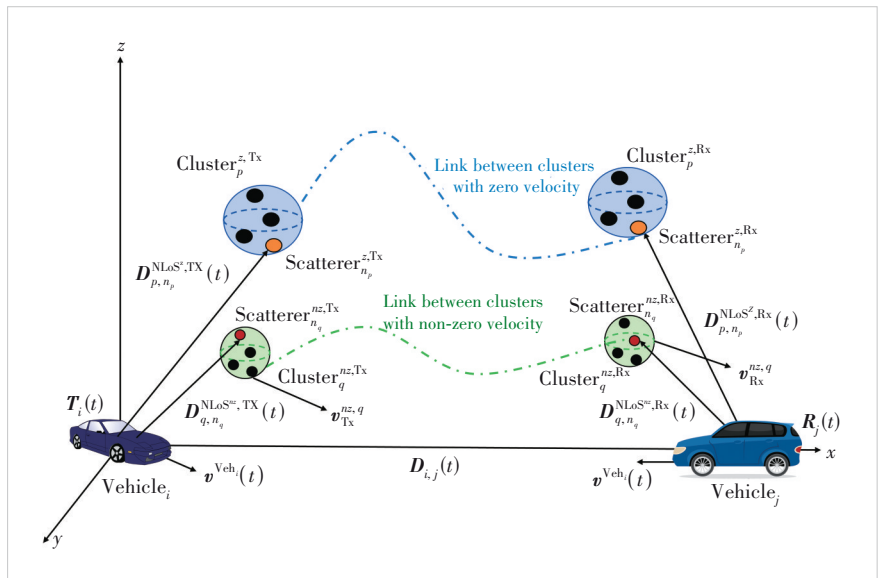


Figure 3. Geometry of the proposed DT-enabled vehicular communication channel model for Beijing CBD

3.1.1 Ground Reflection Component

The ground reflection component complex channel gain of the transmission link from the i -th vehicle to the j -th vehicle can be represented as

$$h^{\text{GR}}(t) = Q(t) \sqrt{P^{\text{GR}}(t)} \times \exp \left\{ j2\pi \left[\int_{t_0}^t f^{\text{GR},V_i}(t) dt + \int_{t_0}^t f^{\text{GR},V_j}(t) dt \right] + j\varphi^{\text{GR}}(t) \right\} \quad (2),$$

where $Q(t)$ is a rectangular window function^[15]; it equals 1 when $t_0 \leq t \leq T_0$ (where T_0 means the observation time interval), otherwise equals 0. $P^{\text{GR}}(t)$, $f^{\text{GR},V_i}(t)$, $\varphi^{\text{GR}}(t)$, and $\tau^{\text{GR}}(t)$ denote power, Doppler frequency at the ij -th vehicle, phase, and delay of the ground reflection component from the i -th vehicle to the j -th vehicle, respectively. The Doppler frequency $f^{\text{GR},V_i/V_j}(t)$ is expressed as

$$f^{\text{GR},V_i/V_j}(t) = \frac{1}{\lambda} \frac{\langle \mathbf{D}^{\text{GR},V_i/V_j}(t), \mathbf{v}^{V_i/V_j}(t) \rangle}{\| \mathbf{D}^{\text{GR},V_i/V_j}(t) \|} \quad (3),$$

where $\mathbf{D}^{\text{GR},V_i/V_j}(t)$ is the distance vector from the ij -th vehicle to the reflection point on the ground. The phase of the ground reflection component from the i -th vehicle to the j -th vehicle can be computed as

$$\varphi^{\text{GR}}(t) = \varphi_0 + \frac{2\pi}{\lambda} \left(\| \mathbf{D}^{\text{GR},V_i}(t) \| + \| \mathbf{D}^{\text{GR},V_j}(t) \| \right) \quad (4),$$

where φ_0 is the initial phase shift.

The delay of the ground reflection component from the i -th vehicle to the j -th vehicle, $\tau^{\text{GR}}(t)$, can be computed as

$$\tau^{\text{GR}}(t) = \frac{\| \mathbf{D}^{\text{GR},V_i}(t) \| + \| \mathbf{D}^{\text{GR},V_j}(t) \|}{c} \quad (5).$$

The calculation of distance vectors $\mathbf{D}^{\text{GR},V_i}(t)$ and $\mathbf{D}^{\text{GR},V_j}(t)$ is expressed below. The azimuth distance between the TX (the i -th vehicle) and the ground reflection point is $d_{V_i}(t)$,

which is derived from $d_{V_i}(t) = \frac{\| \mathbf{D}^{V_i,V_j}(t) \| h_{V_i}(t)}{h_{V_i}(t) + h_{V_j}(t)}$; $h_{V_i}(t)$ and

$h_{V_j}(t)$ are the ground clearances of the i -th vehicle and the j -th vehicle. With the geometrical relationship, the distance between the ij -th vehicle and ground reflection point can be computed as $\| \mathbf{D}^{\text{GR},V_i}(t) \| = \sqrt{d_{V_i}^2(t) + h_{V_i}^2(t)}$ and

$\| \mathbf{D}^{\text{GR},V_j}(t) \| = \sqrt{\| \mathbf{D}^{V_i,V_j}(t) \|^2 + h_{V_i}^2(t) + h_{V_j}^2(t) - \| \mathbf{D}^{\text{GR},V_i}(t) \|^2}$. The corresponding distance vectors can be expressed as

$$\mathbf{D}^{\text{GR},V_i/V_j} = \| \mathbf{D}^{\text{GR},V_i/V_j} \| \times \begin{bmatrix} \cos \alpha^{\text{GR},V_i/V_j}(t) \cos \beta^{\text{GR},V_i/V_j}(t) \\ \sin \alpha^{\text{GR},V_i/V_j}(t) \cos \beta^{\text{GR},V_i/V_j}(t) \\ \sin \beta^{\text{GR},V_i/V_j}(t) \end{bmatrix} \quad (6),$$

where $\alpha^{\text{GR},V_i/V_j}$ and $\beta^{\text{GR},V_i/V_j}$ are the azimuth and elevation angles of the distance vector $\mathbf{D}^{\text{GR},V_i/V_j}$. As the azimuth angle of the ground reflection path matches that of the line-of-sight (LoS) path and the combined power of the LoS and ground reflection paths remains constant, only the elevation angle of the ground reflection path needs to be taken into account similar to Ref [16]. $\beta^{\text{GR},V_i/V_j}$ is computed as $\beta^{\text{GR},V_i/V_j} = \arctan \frac{h_{V_j}}{d_{V_j}(t)}$.

3.1.2 LoS Component

The LoS complex channel gain of the transmission link from the i -th vehicle to the j -th vehicle can be represented as

$$h^{\text{LoS}}(t) = Q(t) \exp \left[j2\pi \int_{t_0}^t f^{\text{LoS}}(t) dt + j\varphi^{\text{LoS}}(t) \right] \quad (7).$$

The Doppler frequency, phase shift, and delay of the LoS component of the transmission link from the i -th vehicle to the j -th vehicle are obtained by

$$f^{\text{LoS}}(t) = \frac{1}{\lambda} \frac{\langle \mathbf{D}^{\text{LoS}}(t), \mathbf{v}^{V_j}(t) - \mathbf{v}^{V_i}(t) \rangle}{\| \mathbf{D}^{\text{LoS}}(t) \|} \quad (8),$$

$$\varphi^{\text{LoS}}(t) = \varphi_0 + \frac{2\pi}{\lambda} \| \mathbf{D}^{\text{LoS}}(t) \| \quad (9),$$

$$\tau^{\text{LoS}}(t) = \frac{\| \mathbf{D}^{\text{LoS}}(t) \|}{c} \quad (10),$$

where $\langle \cdot, \cdot \rangle$, φ_0 , and λ are the inner product, initial phase shift, and carrier wavelength; $\mathbf{v}^{V_i}(t)$ and $\mathbf{v}^{V_j}(t)$ are the velocity vectors of the i -th vehicle and the j -th vehicle. Meanwhile, the distance vector for the i -th vehicle and the j -th vehicle $\mathbf{D}^{\text{LoS}}(t)$ is obtained by

$$\mathbf{D}^{\text{LoS}}(t) = \mathbf{D}^{\text{LoS}}(t_0) + \int_{t_0}^t \mathbf{v}^{V_j}(t) dt - \int_{t_0}^t \mathbf{v}^{V_i}(t) dt \quad (11).$$

3.1.3 Non-LoS Component

Vehicular communication's high mobility causes real-time changes in the communication environment. To characterize the non-line-of-sight (NLoS) component of the channel gain, it is essential to separately model the characteristics of scatterers according to their velocities. To compute the NLoS component's complex channel gain, we separately calculate

the complex channel gains of clusters with zero and non-zero velocities. Using LiDAR point clouds and RGB images, the scatterers are classified by velocity (zero/non-zero). Meanwhile, the scatterer parameters with different velocities will be analyzed and utilized for channel modeling, detailed in the next subsection. To depict the NLoS complex channel gain more clearly, we define clusters with centroids closer to TX/RX as TX/RX clusters, which are then randomly shuffled and paired to create twin clusters. The p -th TX/RX cluster with zero velocity and the q -th TX/RX cluster with non-zero velocity are represented as $C_{\text{TX/RX}}^{z,p}$ and $C_{\text{TX/RX}}^{nz,q}$. The velocity vector $\mathbf{v}_{\text{TX/RX}}^{nz,q}$ is utilized to depict the q -th TX/RX cluster with non-zero velocity.

The NLoS component's complex channel gain from the i -th vehicle and the j -th vehicle via the n_p -th scatterer in the p -th twin cluster with zero velocity, i.e., $h_{\rho,n_p}^{\text{NLoS}^z}(t)$, is calculated by

$$h_{\rho,n_p}^{\text{NLoS}^z}(t) = Q(t) \sqrt{P_{\rho,n_p}^{\text{NLoS}^z}(t)} \times \exp \left\{ j2\pi \left[\int_{t_0}^t f_{\rho,n_p}^{\text{NLoS}^z,\text{TX}}(t) dt + \int_{t_0}^t f_{\rho,n_p}^{\text{NLoS}^z,\text{RX}}(t) dt \right] + j\varphi_{\rho,n_p}^{\text{NLoS}^z}(t) \right\} \quad (12),$$

where $P_{\rho,n_p}^{\text{NLoS}^z}(t)$ is the normalized power of ZVS, $f_{\rho,n_p}^{\text{NLoS}^z,\text{TX/RX}}(t)$ is the Doppler frequency of the clusters with zero velocity at TX/RX, and $\varphi_{\rho,n_p}^{\text{NLoS}^z}(t)$ is the phase shift. $f_{\rho,n_p}^{\text{NLoS}^z,\text{TX/RX}}$ is computed by

$$f_{\rho,n_p}^{\text{NLoS}^z,\text{TX}}(t) = \frac{1}{\lambda} \frac{\langle \mathbf{D}_{\rho,n_p}^{\text{NLoS}^z,\text{TX}}(t), \mathbf{v}^{\text{TX}}(t) \rangle}{\| \mathbf{D}_{\rho,n_p}^{\text{NLoS}^z,\text{TX}}(t) \|} \quad (13),$$

$$f_{\rho,n_p}^{\text{NLoS}^z,\text{RX}}(t) = \frac{1}{\lambda} \frac{\langle \mathbf{D}_{\rho,n_p}^{\text{NLoS}^z,\text{RX}}(t), \mathbf{v}^{\text{RX}}(t) \rangle}{\| \mathbf{D}_{\rho,n_p}^{\text{NLoS}^z,\text{RX}}(t) \|} \quad (14),$$

where $\mathbf{D}_{\rho,n_p}^{\text{NLoS}^z,\text{TX/RX}}(t)$ represents the distance between the TX/RX and the n_p -th scatterer in the p -th twin cluster $C_{\text{TX/RX}}^{z,p}$. The distance $\mathbf{D}_{\rho,n_p}^{\text{NLoS}^z,\text{TX/RX}}(t)$ is given by

$$\mathbf{D}_{\rho,n_p}^{\text{NLoS}^z,\text{TX/RX}}(t) = \begin{pmatrix} \cos \alpha_{\rho,n_p}^{\text{NLoS}^z,\text{TX/RX}}(t) \cos \beta_{\rho,n_p}^{\text{NLoS}^z,\text{TX/RX}}(t) \\ \sin \alpha_{\rho,n_p}^{\text{NLoS}^z,\text{TX/RX}}(t) \cos \beta_{\rho,n_p}^{\text{NLoS}^z,\text{TX/RX}}(t) \\ \sin \beta_{\rho,n_p}^{\text{NLoS}^z,\text{TX/RX}}(t) \end{pmatrix} \quad (15).$$

The phase shift is computed by

$$\varphi_{\rho,n_p}^{\text{NLoS}^z}(t) = \varphi_0 + \frac{2\pi}{\lambda} \left[\| \mathbf{D}_{\rho,n_p}^{\text{NLoS}^z,\text{TX}}(t) \| + \| \mathbf{D}_{\rho,n_p}^{\text{NLoS}^z,\text{RX}}(t) \| + c\tilde{\tau}^{z,p}(t) \right] \quad (16),$$

where $\tilde{\tau}^{z,p}(t)$ represents the delay of the virtual link between the twin clusters $C_{\text{TX/RX}}^{z,p}$, which obeys the Exponential distribution. Moreover, the delay via clusters with zero velocity at TX/RX is computed by

$$\tau_{\rho,n_p}^{\text{NLoS}^z}(t) = \frac{\| \mathbf{D}_{\rho,n_p}^{\text{NLoS}^z,\text{TX}}(t) \| + \| \mathbf{D}_{\rho,n_p}^{\text{NLoS}^z,\text{RX}}(t) \|}{c} + \tilde{\tau}^{z,p}(t) \quad (17).$$

Similarly, the NLoS complex channel gain from the i -th vehicle and the j -th vehicle via the n_q -th scatterer in the q -th twin cluster with non-zero velocity, i.e., $h_{q,n_q}^{\text{NLoS}^{nz}}(t)$, is calculated by

$$h_{q,n_q}^{\text{NLoS}^{nz}}(t) = Q(t) \sqrt{P_{q,n_q}^{\text{NLoS}^{nz}}(t)} \times \exp \left\{ j2\pi \left[\int_{t_0}^t f_{q,n_q}^{\text{NLoS}^{nz},\text{TX}}(t) dt + \int_{t_0}^t f_{q,n_q}^{\text{NLoS}^{nz},\text{RX}}(t) dt \right] + j\varphi_{q,n_q}^{\text{NLoS}^{nz}}(t) \right\} \quad (18),$$

where $P_{q,n_q}^{\text{NLoS}^{nz}}(t)$ is the normalized power of NVS, $f_{q,n_q}^{\text{NLoS}^{nz},\text{TX/RX}}(t)$ is the Doppler frequency of the clusters with non-zero velocity at TX/RX, and $\varphi_{q,n_q}^{\text{NLoS}^{nz}}(t)$ is the phase shift. $f_{q,n_q}^{\text{NLoS}^{nz},\text{TX/RX}}$ is computed by

$$f_{q,n_q}^{\text{NLoS}^{nz},\text{TX}}(t) = \frac{1}{\lambda} \frac{\langle \mathbf{D}_{q,n_q}^{\text{NLoS}^{nz},\text{TX}}(t), \mathbf{v}^{\text{TX}}(t) \rangle}{\| \mathbf{D}_{q,n_q}^{\text{NLoS}^{nz},\text{TX}}(t) \|} \quad (19),$$

$$f_{q,n_q}^{\text{NLoS}^{nz},\text{RX}}(t) = \frac{1}{\lambda} \frac{\langle \mathbf{D}_{q,n_q}^{\text{NLoS}^{nz},\text{RX}}(t), \mathbf{v}^{\text{RX}}(t) \rangle}{\| \mathbf{D}_{q,n_q}^{\text{NLoS}^{nz},\text{RX}}(t) \|} \quad (20),$$

where $\mathbf{D}_{q,n_q}^{\text{NLoS}^{nz},\text{TX/RX}}(t)$ represents the distance between the TX/RX and the n_q -th scatterer in the q -th twin cluster $C_{\text{TX/RX}}^{nz,q}$. The distance $\mathbf{D}_{q,n_q}^{\text{NLoS}^{nz},\text{TX/RX}}(t)$ is given by

$$\mathbf{D}_{q,n_q}^{\text{NLoS}^{nz},\text{TX/RX}}(t) = \begin{pmatrix} \cos \alpha_{q,n_q}^{\text{NLoS}^{nz},\text{TX/RX}}(t) \cos \beta_{q,n_q}^{\text{NLoS}^{nz},\text{TX/RX}}(t) \\ \sin \alpha_{q,n_q}^{\text{NLoS}^{nz},\text{TX/RX}}(t) \cos \beta_{q,n_q}^{\text{NLoS}^{nz},\text{TX/RX}}(t) \\ \sin \beta_{q,n_q}^{\text{NLoS}^{nz},\text{TX/RX}}(t) \end{pmatrix} \quad (21).$$

The phase shift is computed by

$$\varphi_{q,n_q}^{\text{NLoS}^{nz}}(t) = \varphi_0 + \frac{2\pi}{\lambda} \left[\left\| \mathbf{D}_{q,n_q}^{\text{NLoS}^{nz},\text{TX}}(t) \right\| + \left\| \mathbf{D}_{q,n_q}^{\text{NLoS}^{nz},\text{RX}}(t) \right\| + c\tilde{\tau}^{nz,q}(t) \right] \quad (22),$$

where $\tilde{\tau}^{nz}(t)$ represents the delay of the virtual link between the twin clusters $C_{\text{TX/RX}}^{nz,q}$, which also obeys the Exponential distribution. Moreover, the delay via clusters with non-zero velocity at TX/RX is computed by

$$\tau_{q,n_q}^{\text{NLoS}^{nz}}(t) = \frac{\left\| \mathbf{D}_{q,n_q}^{\text{NLoS}^{nz},\text{TX}}(t) \right\| + \left\| \mathbf{D}_{q,n_q}^{\text{NLoS}^{nz},\text{RX}}(t) \right\|}{c} + \tilde{\tau}^{nz,q}(t) \quad (23).$$

The power parameter $P_{plq,n_{plq}}^{\text{NLoS}^{nz}}(t)$, distance parameter $D_{plq,n_{plq}}^{\text{NLoS}^{nz},\text{TX/RX}}(t)$, and angle parameters $\alpha_{plq,n_{plq}}^{\text{NLoS}^{nz},\text{TX/RX}}(t)$ and $\beta_{plq,n_{plq}}^{\text{NLoS}^{nz},\text{TX/RX}}(t)$ obey different statistical distributions, which are analyzed in the following subsection.

3.2 Parameters for Channel Realization

Based on the constructed DT-based Beijing CBD vehicular communication dataset, we use statistical approaches to compute the distribution of parameters related to scatterers with different velocities.

Accurately characterizing and modeling the number of scatterers and clusters is crucial for channel models^[17]. However, the statistical properties of the corresponding scatterers/clusters are not depicted in the current standardized models for scatterers with different velocities^[18-19]. To comprehensively characterize vehicular communication channels in Beijing CBD, the quantities of scatterers/clusters with zero/non-zero velocities are explored. The numbers of ZVS and NVS in the transmission link from the i -th vehicle (TX) to the j -th vehicle (RX) are denoted as $N_{s_{ij}}^z(t)$ and $N_{s_{ij}}^{nz}(t)$. Since the distance between the transceivers affects the evaluation of the scatterer number, the parameters controlling scatterer numbers are defined as $Y_{i,j}^z$ and $Y_{i,j}^{nz}$, which can be represented as

$$Y_{i,j}^z(t) = \frac{N_{s_{ij}}^z(t)}{\left\| \mathbf{T}_i(t) - \mathbf{R}_j(t) \right\|} \quad (24),$$

$$Y_{i,j}^{nz}(t) = \frac{N_{s_{ij}}^{nz}(t)}{\left\| \mathbf{T}_i(t) - \mathbf{R}_j(t) \right\|} \quad (25),$$

where $\mathbf{T}_i(t)$ and $\mathbf{R}_j(t)$ are the locations of the i -th and j -th vehicles. Moreover, based on the constructed DT-based Beijing CBD vehicular communication dataset, the number ratios of ZVS and NVS for each communication link per snapshot across peak and off-peak traffic periods are calculated and analyzed. Fig. 4 presents the cumulative distribution functions (CDFs) of the velocity-based ratio related to the scatterer number during peak and off-peak hours. These CDFs fit well with the Gaussian mixture model (GMM), which can be

represented as

$$F_Y^{z/nz}(x) = \sum_{k=1}^{K^{z/nz}} \pi_k^{z/nz} \mathcal{F}_{Y,k}^{z/nz}(x) \quad (26),$$

where $\mathcal{F}_{Y,k}^{z/nz}(x)$ and $\pi_k^{z/nz}$ are the CDF and weight of the k -th Gaussian distribution, respectively. $\mathcal{F}_{Y,k}^{z/nz}(x)$ can be given by

$$\mathcal{F}_{Y,k}^{z/nz}(x) = \Phi_{Y,k}^{z/nz} \left(\frac{x - \mu_{Y,k}^{z/nz}}{\sigma_{Y,k}^{z/nz}} \right),$$

where $\Phi_{Y,k}^{z/nz}$ is the CDF of the standard normal distribution; $\mu_{Y,k}^{z/nz}$ and $\sigma_{Y,k}^{z/nz}$ are the mean and standard deviations of the k -th Gaussian distribution. The ratios related to scatterer numbers can be obtained from the simulations using the constructed DT-based Beijing CBD vehicular communication dataset. The number of Gaussian distributions k is 3. During off-peak hours, the simulation parameters for the ZVS are $\pi_k^z = [0.3952; 0.4666; 0.1382]$, $\mu_{Y,k}^z = [0.1565; 0.0263; 0.6179]$, and $\sigma_{Y,k}^z = [0.0082; 3.63 \times 10^{-4}; 0.1912]$, while those for the NVS are $\pi_k^{nz} = [0.1148; 0.3175; 0.5677]$, $\mu_{Y,k}^{nz} = [0.1164; 0.0492; 0.0107]$ and $\sigma_{Y,k}^{nz} = [0.0016; 5.14 \times 10^{-4}; 3.21 \times 10^{-5}]$. Meanwhile, during peak hours, the simulation parameters for the ZVS are $\pi_k^z = [0.3504; 0.2819; 0.3677]$, $\mu_{Y,k}^z = [1.1673; 0.4263; 0.0723]$, and $\sigma_{Y,k}^z = [0.2542; 0.0222; 0.0029]$, while those for the NVS are $\pi_k^{nz} = [0.6034; 0.3784; 0.0182]$, $\mu_{Y,k}^{nz} = [0.0115; 0.0558; 0.2735]$, and $\sigma_{Y,k}^{nz} = [2.94 \times 10^{-5}; 3.86 \times 10^{-4}; 0.0089]$. Fig. 4 shows that both the mean and variance of the number-related parameters for the NVS are greater during peak hours than during off-peak hours. This is because there are more dynamic vehicles around the transceiver during peak

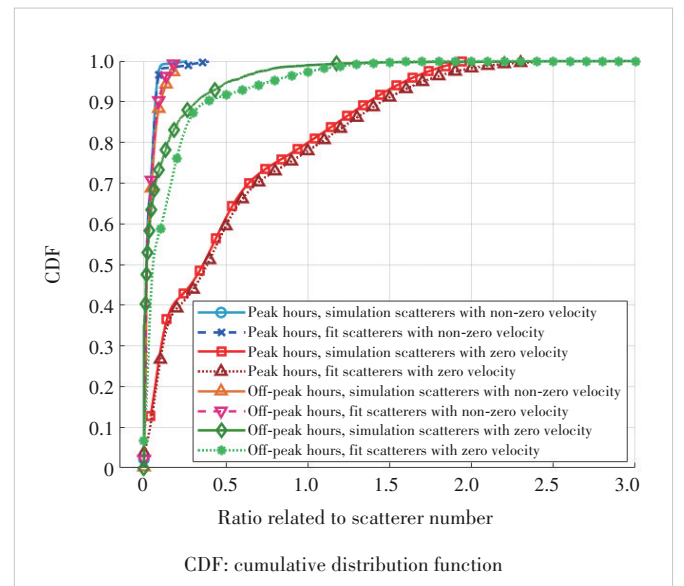


Figure 4. GMM-fitted CDFs of velocity-based ratios related to scatterer numbers during peak and off-peak hours

hours, which increases the number of NVS. For the ZVS, the mean and variance are also greater during peak hours than during off-peak hours. This is due to the fact that the environment tends to be rich scattering during peak hours, resulting in more propagation paths.

To investigate vehicular channel characteristics in Beijing CBD in detail, the scatterers are clustered to analyze cluster population statistics. Therefore, the parameters of zero-velocity and non-zero-velocity clusters in the transmission link from the i -th vehicle (TX) to the j -th vehicle (RX) are denoted as $U_{i,j}^z$ and $U_{i,j}^{nz}$. For each communication link per snapshot, we denote the velocity-based cluster-number parameters across peak and off-peak hours. The CDFs of velocity-based ratios related to cluster numbers follow GMM distributions, which can be expressed as

$$F_U^{z/nz}(x) = \sum_{k=1}^{K^{z/nz}} \pi_k^{z/nz} \mathcal{F}_{U,k}^{z/nz}(x) \quad (27),$$

where $\mathcal{F}_{U,k}^{z/nz}(x)$, the CDF of the k -th Gaussian distribution, can be given by $\mathcal{F}_{U,k}^{z/nz}(x) = \Phi_{U,k}^{z/nz}\left(\frac{x - \mu_{U,k}^{z/nz}}{\sigma_{U,k}^{z/nz}}\right)$, where $\Phi_{U,k}^{z/nz}$ is the

CDF of the standard normal distribution, while $\mu_{U,k}^{z/nz}$ and $\sigma_{U,k}^{z/nz}$ are the mean and standard deviations of the k -th Gaussian distribution. The number of Gaussian distributions k is also 3. For the clusters with zero velocity during off-peak hours, the simulation parameters are $\pi_k^z = [0.254\ 3; 0.631\ 5; 0.114\ 2]$, $\mu_{U,k}^z = [0.040\ 9; 0.010\ 3; 0.101\ 7]$, and $\sigma_{U,k}^z = [2.97 \times 10^{-4}; 4.76 \times 10^{-5}; 0.002]$. As for the clusters with non-zero velocity during off-peak hours, the parameters are $\pi_k^{nz} = [0.298\ 4; 0.606\ 8; 0.094\ 8]$, $\mu_{U,k}^{nz} = [0.551\ 5; 0.011\ 7; 0.109\ 7]$, and $\sigma_{U,k}^{nz} = [2.36 \times 10^{-4}; 3.05 \times 10^{-5}; 0.001\ 7]$. Meanwhile, for the clusters with zero velocity during peak hours, the simulation parameters are $\pi_k^z = [0.340\ 6; 0.401\ 9; 0.257\ 5]$, $\mu_{U,k}^z = [0.085\ 2; 0.020\ 0; 0.212\ 0]$ and $\sigma_{U,k}^z = [6.96 \times 10^{-4}; 1.17 \times 10^{-4}; 0.005\ 5]$. For the clusters with non-zero velocity during peak hours, the parameters are $\pi_k^{nz} = [0.195\ 2; 0.778\ 5; 0.026\ 3]$, $\mu_{U,k}^{nz} = [0.033\ 3; 0.010\ 9; 0.065\ 6]$, and $\sigma_{U,k}^{nz} = [2.01 \times 10^{-5}; 3.01 \times 10^{-5}; 1.07 \times 10^{-5}]$. Fig. 5 presents the CDFs of the velocity-based ratios related to cluster numbers during peak and off-peak hours. The parameters related to the cluster number show similar trends to those related to the scatterer number with different velocities during peak and off-peak hours.

Distance distribution of scatterers is important for stochastic channel modeling. The distance parameters of scatterers are assumed to follow the Exponential distribution in Ref. [20]. However, scatterer velocity variations and traffic density differences during peak and off-peak hours are ignored. Based on the constructed DT-based Beijing CBD vehicular communication dataset, distance characteristics of the scatterers with different velocities are explored. The distance pa-

rameters for the m -th scatterer with zero velocity and the n -th scatterer with non-zero velocity from the transceiver, i.e., the i -th vehicle and the j -th vehicle, are represented as

$$D_{i,j}^{z,m}(t) = \frac{\|T_i(t) - S_{i,j}^{z,m}(t)\| + \|R_j(t) - S_{i,j}^{z,m}(t)\| - \|T_i(t) - R_j(t)\|}{\|T_i(t) - R_j(t)\|} \quad (28),$$

$$D_{i,j}^{nz,n}(t) = \frac{\|T_i(t) - S_{i,j}^{nz,n}(t)\| + \|R_j(t) - S_{i,j}^{nz,n}(t)\| - \|T_i(t) - R_j(t)\|}{\|T_i(t) - R_j(t)\|} \quad (29),$$

where $S_{i,j}^{z,m}(t)$ and $S_{i,j}^{nz,n}(t)$ are the locations of the m -th scatterer with zero velocity and the n -th scatterer with non-zero velocity in the transmission link between the i -th vehicle and the j -th vehicle; $\|\cdot\|$ denotes the calculation of the Frobenius norm. We compute the distance parameters of scatterers with different velocities during peak and off-peak hours for each communication link per snapshot. The CDFs of distance parameters with different velocities also fit well with the GMM distribution, which is represented as

$$F_D^{z/nz}(x) = \sum_{k=1}^{K^{z/nz}} \pi_k^{z/nz} \mathcal{F}_{D,k}^{z/nz}(x) \quad (30),$$

where $\mathcal{F}_{D,k}^{z/nz}(x)$, the CDF of the k -th Gaussian distribution, can be given by $\mathcal{F}_{D,k}^{z/nz}(x) = \Phi_{D,k}^{z/nz}\left(\frac{x - \mu_{D,k}^{z/nz}}{\sigma_{D,k}^{z/nz}}\right)$, where $\Phi_{D,k}^{z/nz}$ is the CDF of the standard normal distribution, and $\mu_{D,k}^{z/nz}$ and $\sigma_{D,k}^{z/nz}$

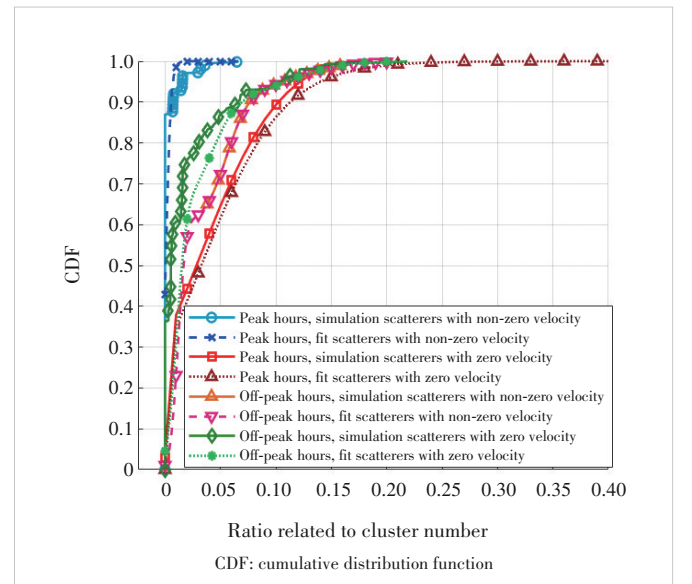


Figure 5. GMM-fitted CDFs of velocity-based ratios related to cluster numbers during peak and off-peak hours

are the mean and standard deviations of the k -th Gaussian distribution. The number of Gaussian distributions k is still 3. During off-peak hours, the simulation parameters for ZVS are $\pi_k^z = [0.3129; 0.5474; 0.1397]$, $\mu_{D,k}^z = [7.7240; 0.6530; 20.9916]$, and $\sigma_{ND,k}^z = [9.6283; 0.3164; 102.07]$, while the parameters for the NVS are $\pi_k^{nz} = [0.6742; 0.2392; 0.0688]$, $\mu_{D,k}^{nz} = [0.7105; 6.8795; 20.9435]$, and $\sigma_{D,k}^{nz} = [0.5127; 10.7507; 93.2294]$. On the other hand, during peak hours, the simulation parameters for the ZVS are $\pi_k^z = [0.6231; 0.1267; 0.2502]$, $\mu_{D,k}^z = [0.6898; 27.9952; 7.3956]$, and $\sigma_{D,k}^z = [0.4437; 110.2286; 6.6734]$, while the parameters for the NVS are $\pi_k^{nz} = [0.7360; 0.0125; 0.2515]$, $\mu_{D,k}^{nz} = [0.5199; 4.9894; -0.0932]$ and $\sigma_{D,k}^{nz} = [0.0373; 0.0030; 0.0015]$. Fig. 6 shows the CDFs of all distance parameters of the scatterers with different velocities during peak and off-peak hours. The distance parameter of ZVS is larger than that of NVS during peak and off-peak hours, as ZVSes are mainly tall buildings and trees, while NVSes are dynamic vehicles. Dynamic vehicles are generally closer to the TX and RX, which leads to a shorter distance. The variance of the distance parameter is smaller at peak hours than that at off-peak hours since the scatterer distribution is more centered as vehicles around the transceiver increase.

The angle parameters related to scatterers are also crucial for analyzing and constructing channel models for DT-enabled vehicular communication within Beijing CBD. These parameters, including azimuth angle of departure (AAoD), azimuth angle of arrival (AAoA), elevation angle of departure (EAoD), and elevation angle of arrival (EAoA), are analyzed

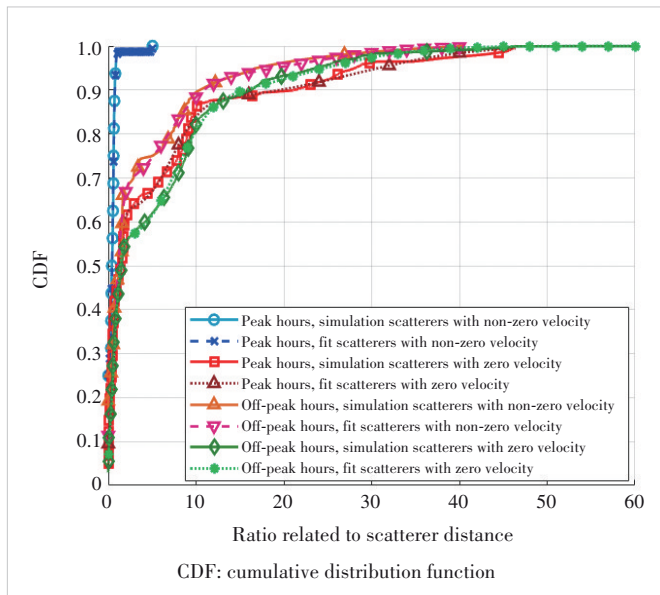


Figure 6. GMM-fitted CDFs of distance parameters during peak and off-peak hours

for the scatterers with different velocities under different traffic densities during peak and off-peak hours. AAoA ratios for the m -th scatterer with zero velocity and the n -th scatterer with non-zero velocity from the transceiver, i.e., the i -th vehicle and the j -th vehicle, are expressed as

$$\alpha_{i,j}^{z,m}(t) = \frac{\gamma_{i,j}^{z,m}(t)}{\|T_i(t) - R_i(t)\|} \quad (31),$$

$$\alpha_{i,j}^{nz,n}(t) = \frac{\gamma_{i,j}^{nz,n}(t)}{\|T_i(t) - R_i(t)\|} \quad (32),$$

where $\gamma_{i,j}^{z,m}(t)$ and $\gamma_{i,j}^{nz,n}(t)$ represent the AAoAs of the m -th scatterer with zero velocity and the n -th scatterer with non-zero velocity from the transceiver. Furthermore, based on the DT-based Beijing CBD vehicular communication dataset, the AAoAs of scatterers with different velocities in each communication link per snapshot are analyzed. Fig. 7 shows the CDFs of all AAoAs of the scatterers with different velocities under different traffic densities during peak and off-peak hours, which fit well with the Gaussian distribution. The CDF of the Gaussian distribution for AAoAs related to scatterers with different velocities can be represented by

$$F_{AAoA}^z(x) = \frac{1}{2} \left[1 + \operatorname{erf} \left(\frac{x - \mu_{AAoA}^z}{\sigma_{AAoA}^z \sqrt{2}} \right) \right] \quad (33),$$

$$F_{AAoA}^{nz}(x) = \frac{1}{2} \left[1 + \operatorname{erf} \left(\frac{x - \mu_{AAoA}^{nz}}{\sigma_{AAoA}^{nz} \sqrt{2}} \right) \right] \quad (34),$$

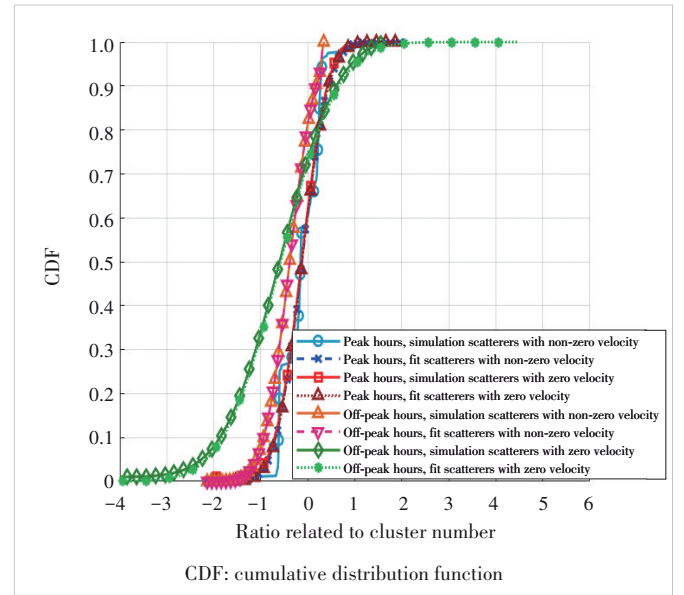


Figure 7. Gaussian-fitted CDFs of azimuth angle of departure (AAoD) during peak and off-peak hours

where $\mu_{AAoA}^{z/nz}$ and $\sigma_{AAoA}^{z/nz}$ denote the mean value and standard deviation of the Gaussian distribution for AAoAs related to scatterers with different velocities; $\text{erf}(\cdot)$ is the error function. Similarly, AAoD $\theta_{i,j}^{z/nz,m/n}(t)$, EAoA $\beta_{i,j}^{z/nz,m/n}(t)$, and EAoD $\phi_{i,j}^{z/nz,m/n}(t)$ are calculated and also obey the Gaussian distribution. The distance parameters of the simulation during off-peak hours are $\mu_{AAoA}^{z/nz} = -0.5769/ -0.3852$, $\sigma_{AAoA}^{z/nz} = 1.065/0.4335$; $\mu_{AAoD}^{z/nz} = -0.1464/0.2968$, $\sigma_{AAoD}^{z/nz} = 1.2974/0.9008$; $\mu_{EAoA}^{z/nz} = -0.1294/ -0.0293$, $\sigma_{EAoA}^{z/nz} = 0.1539/0.0367$; $\mu_{EAoD}^{z/nz} = -0.1579/ -0.0523$, $\sigma_{EAoD}^{z/nz} = 0.2890/0.0664$, while the distance parameters during peak hours are $\mu_{AAoA}^{z/nz} = -0.5481/ -0.1221$, $\sigma_{AAoA}^{z/nz} = 1.0811/0.4349$; $\mu_{AAoD}^{z/nz} = -0.1640/0.2126$, $\sigma_{AAoD}^{z/nz} = 1.2372/0.8910$; $\mu_{EAoA}^{z/nz} = -0.1468/ -0.0698$, $\sigma_{EAoA}^{z/nz} = 0.1655/0.1038$; $\mu_{EAoD}^{z/nz} = -0.2267/ -0.1901$, $\sigma_{EAoD}^{z/nz} = 0.4810/0.6301$. As shown in Fig. 7 and according to the angle parameters of the statistical distributions above, NVS have a smaller azimuth angle variance than those with zero velocity. This is because the NVS mainly come from dynamic vehicles, which have less variation in heights. Moreover, the angle parameter variance is larger during peak hours than during off-peak hours. This is due to the more complex and variable environment during peak hours, causing greater angle variations.

In addition, path power and delay characteristics are significant in channel realization. The path power is an exponential function of the path delay^[21]. Using the DT-based Beijing CBD vehicular communication dataset, we separate the path power into power via ZVS and that via NVS. The path power from the i -th vehicle to the j -th vehicle via the m -th scatterer with zero velocity and the n -th scatterer with non-zero velocity is expressed by

$$P^{z,m}(t) = \exp\left(-\xi^z \tau^{z,m}(t) - \eta^z\right) 10^{-\frac{Z^z}{10}} \quad (35),$$

$$P^{nz,n}(t) = \exp\left(-\xi^{nz} \tau^{nz,n}(t) - \eta^{nz}\right) 10^{-\frac{Z^{nz}}{10}} \quad (36),$$

where $\xi^{z/nz}$ and $\eta^{z/nz}$ are the delay-related parameters of scatterers with different velocities; $\tau^{z/nz,m/n}$ is the delay of the path via the m -th scatterer with zero velocity and the n -th scatterer with non-zero velocity; $Z^{z/nz}$ follows the Gaussian distribution $\mathcal{N}\left(0, (\sigma_E^{z/nz})^2\right)$. For accurate linear fitting, Eqs. (35) and (36) are transformed as

$$-\ln P^{z,m}(t) = \xi^z \tau^{z,m}(t) + \eta^z + \frac{\ln 10}{10} Z^z \quad (37),$$

$$-\ln P^{nz,n}(t) = \xi^{nz} \tau^{nz,n}(t) + \eta^{nz} + \frac{\ln 10}{10} Z^{nz} \quad (38).$$

The power and delay of each path via each scatterer with different velocities per snapshot are calculated. Fig. 8 pres-

ents the fitting results under different traffic densities during peak and off-peak hours. The parameters related to power and delay during off-peak hours are $\xi^{z/nz} = 3.7264 \times 10^6/2.7636 \times 10^6$, $\eta^{z/nz} = 28.0658/28.8769$, and $\sigma_E^{z/nz} = 7.9716/7.0059$, while those during peak hours are $\xi^{z/nz} = 4.0294 \times 10^6/2.6133 \times 10^6$, $\eta^{z/nz} = 27.4438/29.4041$, and $\sigma_E^{z/nz} = 8.4828/7.5142$. Fig. 8 shows that the power of NVS is more sensitive to delay changes than that of ZVS. Therefore, an increase in the delay of NVS notably reduces their power.

Consequently, the parameters related to scatterers with different velocities can be generated by the statistical distribution obtained from the aforementioned analysis.

3.3 Capturing of DT-Enabled Channel Non-Stationarity and Consistency

We depict channel non-stationarity and consistency based on the proposed DT-enabled Beijing CBD vehicular communication channel model. The environment is constantly changing with the continuous movement of the vehicle, which leads to continuous changes in LiDAR point clouds and RGB images captured by sensors. Meanwhile, the scatterers in communication links are not effective as they move away from the transceiver. In the transmission links related to different vehicles, the sets of effective clusters are different as well, which leads to the non-stationarity of clusters in the time domain in the DT-enabled Beijing CBD vehicular communication channel. In addition, given the temporal continuity of the communication environment, scatterers exhibit smooth transitions in appearance and disappearance across time and space. This maintains the scatterer consistency in both time and space domains of the DT-enabled Beijing CBD

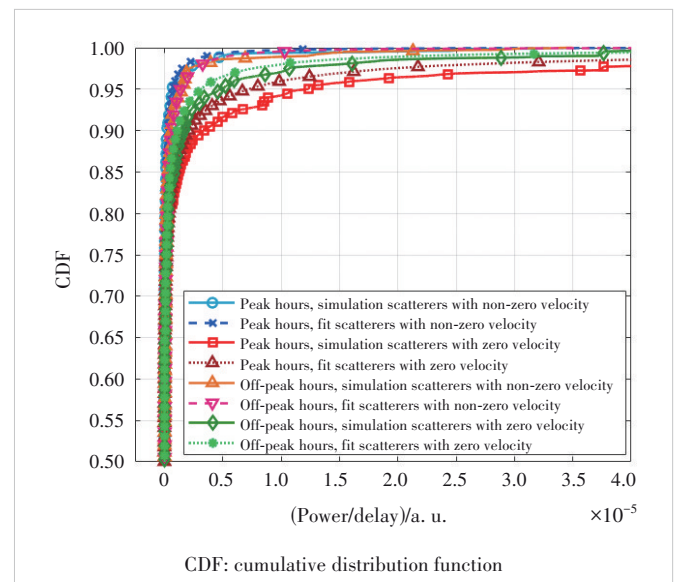


Figure 8. Scatterer power-delay CDFs with Exponential fit during peak and off-peak hours

vehicular communication channel.

To accurately and simultaneously model the channel non-stationarity and consistency in the time domain, a new visibility region (VR)-based method is proposed, which considers the generation of scatterers with different velocities. In the VR methods in Ref. [22], clusters located within the VR range have an impact on the channel realization. As the VR and cluster positions move, the set of visible clusters evolves smoothly, which reflects the channel non-stationarity and consistency in the time domain. To depict smooth cluster time evolution in channels for DT-enabled Beijing CBD vehicular communication, a VR-based method is proposed based on the statistical parameter distribution for different traffic densities during peak and off-peak hours. The scatterers in the environment are initialized, and their parameters, including velocities for peak and off-peak hours, are generated according to the distribution obtained in Section 3.2. The number of scatterers with different velocities between the i -th vehicle and the j -th vehicle at the initial time t_0 and the distances are both generated according to the GMM distribution. The departure and arrival angles (AAoDs, AAoAs, EAoDs, and EAoAs) are generated following the Gaussian distribution. Based on the generated distances and angles for each scatterer, the initial positions of these scatterers at time t_0 are determined. Moreover, the generated scatterers with different velocities are clustered using the K-means algorithm. Each vehicle's VR is modeled as a semi-sphere centered at the vehicle. The VR radius R_i/R_j of the ij -th vehicle is the maximum distance between the vehicle and initially generated velocity-varying clusters at the initial time. The clusters within R_i/R_j at time t are defined as visible clusters. Since the distance between the cluster and TX/RX at time $t_0 + \Delta t$ is still shorter than the radii of VRs, the cluster is still in the VRs and affects the channel. The number of surviving clusters with different velocities between the i -th and j -th vehicles at time $t_0 + \Delta t$ is given as $U_{i,j}^{z,\text{sur}}(t_0 + \Delta t)/U_{i,j}^{z,\text{sur}}(t_0 + \Delta t)$. In addition to the surviving clusters, there are some newly generated clusters with different velocities at time $t_0 + \Delta t$. For a certain distance between the i -th and j -th vehicles at time $t_0 + \Delta t$, the number parameter $U_{i,j}^{z,\text{GMM}}(t_0 + \Delta t)/U_{i,j}^{z,\text{GMM}}(t_0 + \Delta t)$ related to clusters with different velocities is randomly generated according to the GMM distribution. The number of newly generated clusters is computed by

$$U_{i,j}^{z/nz,\text{new}}(t) = U_{i,j}^{z/nz,\text{GMM}}(t) - U_{i,j}^{z/nz,\text{sur}}(t) \quad (39),$$

where $U_{i,j}^{z/nz,\text{GMM}}(t)$ is greater than $U_{i,j}^{z/nz,\text{sur}}(t)$ and there are $U_{i,j}^{z/nz}(t) = U_{i,j}^{z/nz,\text{GMM}}(t)$ clusters with different velocities that contribute to channel realization. However, if $U_{i,j}^{z/nz,\text{GMM}}(t)$ is less than $U_{i,j}^{z/nz,\text{sur}}(t)$, the number of newly generated clusters is $U_{i,j}^{z/nz,\text{new}}(t) = 0$. In this case, there are $U_{i,j}^{z/nz}(t) = U_{i,j}^{z/nz,\text{sur}}(t)$ clusters with different velocities that

contribute to channel realization.

4 Channel Statistical Properties

In this section, the key statistical properties for the proposed DT-enabled Beijing CBD vehicular communication channel are derived, including the TF-CF and DPSD.

4.1 TF-CF

The TF-CF of the transmission from the i -th vehicle to the j -th vehicle can be calculated as

$$\Pi(t, f; \Delta t, \Delta f) = \mathbb{E}[h^*(t, f)h(t + \Delta t, f + \Delta f)] \quad (40),$$

where $\mathbb{E}[\cdot]$ and $(\cdot)^*$ represent the expectation operation and complex conjugate operation similar to Ref. [23]. As the TF-CFs of the LoS component, ground reflection component, and NLoS component can be assumed as independent, the TF-CF can be obtained by

$$\Pi(t, f; \Delta t, \Delta f) = \Pi^{\text{LoS}}(t, f; \Delta t, \Delta f) + \Pi^{\text{GR}}(t, f; \Delta t, \Delta f) + \Pi^{\text{NLoS}^{\text{r}}}(t, f; \Delta t, \Delta f) + \Pi^{\text{NLoS}^{\text{w}}}(t, f; \Delta t, \Delta f) \quad (41).$$

The TF-CFs of the LoS component, ground reflection component, and NLoS component can be computed by

$$\begin{aligned} \Pi^{\text{LoS}}(t, f; \Delta t, \Delta f) = & \sqrt{\frac{\Omega(t)\Omega(t + \Delta t)}{(\Omega(t) + 1)(\Omega(t + \Delta t) + 1)}} h^{\text{LoS}*}(t)h^{\text{LoS}}(t + \\ & \Delta t) \exp[j2\pi f\tau^{\text{LoS}}(t) - (f + \Delta f)\tau^{\text{LoS}}(t + \Delta t)] \end{aligned} \quad (42),$$

$$\begin{aligned} \Pi^{\text{GR}}(t, f; \Delta t, \Delta f) = & \sqrt{\frac{\eta^{\text{GR}}(t)\eta^{\text{GR}}(t + \Delta t)}{(\Omega(t) + 1)(\Omega(t + \Delta t) + 1)}} h^{\text{GR}*}(t)h^{\text{GR}}(t + \\ & \Delta t) \exp[j2\pi f\tau^{\text{GR}}(t) - (f + \Delta f)\tau^{\text{GR}}(t + \Delta t)] \end{aligned} \quad (43),$$

$$\begin{aligned} \Pi^{\text{NLoS}^{\text{w}}}(t, f; \Delta t, \Delta f) = & \sqrt{\frac{\eta^{z/nz}(t)\eta^{z/nz}(t + \Delta t)}{(\Omega(t) + 1)(\Omega(t + \Delta t) + 1)}} \times \\ & \mathbb{E} \left[\sum_{p'l'q'=1}^{N^{z/nz}(t)N^{z/nz}(t + \Delta t)} \sum_{p'l'q'=1}^{N^{z/nz}(t)N^{z/nz}(t + \Delta t)} h_{p'l'q',n_{p'l'q'}}^{z/nz}(t)h_{p'l'q',n_{p'l'q'}}^{z/nz}(t + \Delta t) \times \right. \\ & \left. \exp(j2\pi\tau_{p'l'q',n_{p'l'q'}}^{z/nz}(t)f - (f + \Delta f)\tau_{p'l'q',n_{p'l'q'}}^{z/nz}(t + \Delta t)) \right] \end{aligned} \quad (44).$$

Therefore, the time auto-correlation function (TACF) and the frequency correlation function (FCF) can be obtained by setting $\Delta f = 0$ and $\Delta t = 0$, respectively.

4.2 DPSD

The DPSD can be obtained by the Fourier transform of the TACF, which is computed by

$$\Psi(t; f_D) = \int_{-\infty}^{+\infty} \Pi(t; \Delta t) e^{-j2\pi f_D \Delta t} d(\Delta t) \quad (45),$$

where f_D and $\Pi(t; \Delta t)$ are the Doppler frequency and TACF. The time-varying DPSD depicts the time-varying characteristic of the proposed DT-enabled Beijing CBD vehicular communication channel model.

4.3 Simulation Results and Analysis

The computational complexity of channel modeling mainly focuses on the generation of the CIR matrix. The primary source of computational complexity comes from the calculation of physical environment parameters. Specifically, the time complexity of generating the CIR matrix is $\mathcal{O}(N_t \cdot N_r)$, where N_t and N_r represent the numbers of TXes and RXes, respectively. The time complexity of processing the LiDAR point cloud is $\mathcal{O}(P)$, where P is the number of points in the point clouds. The time complexity of RGB can be considered to be constants in a snapshot of data processing, i.e., $\mathcal{O}(1)$. Therefore, the overall complexity is $\mathcal{O}(N_t \cdot N_r + P)$. The time consumption of the computation mainly depends on the simulation setting.

Key statistical channel properties are simulated and compared with the accurate RT-based results. The parameters remain unchanged unless otherwise stated. The carrier frequency is $f_c = 5.9$ GHz with 20 MHz communication bandwidth. Delays of virtual links $\tau_i(t)$ and $\tau_j(t)$ obey the Exponential distribution with the mean and variance of 80 ns and 15 ns to imitate the complex transmission between twin clusters.

Fig. 9 shows the absolute normalized TACFs during peak and off-peak hours at $t = 0$ s and $t = 5$ s. The TACFs depend on time instants and time separations. Moreover, time non-stationarity is depicted. The TACF decreases as the traffic density increases, demonstrating that the TACF is lower during peak hours than that during off-peak hours. This is because, as the number of vehicles increases, the channel becomes more variable and the temporal correlation decreases.

The RT-based CIRs are collected in Wireless InSite within the DT space shown in Fig. 1. DPSD is derived based on the CIR data compared with the simulated DPSD during peak and off-peak hours. As shown in Fig. 10, the RT-based DPSD is much closer to the simulated DPSD during peak and off-peak hours, which demonstrates the validity of the proposed model. The DPSD is flatter during peak hours than during off-peak hours, because vehicles are denser during peak hours and the vehicular communication channels are more complex. Therefore, the comparison of different traffic densities during peak and off-peak hours is signifi-

cant for the proposed DT-enabled vehicular communication channel model.

The effectiveness of the proposed DT-enabled vehicular communication channel model is demonstrated by comparing the TACF and DPSD of the proposed model with the RT-based TACF and DPSD. In the future, we can analyze more channel characteristics, e. g., angular/delay power spectral densities (PSDs) and root mean square (RMS) angular/Doppler/delay spreads, similar to Ref. [24], to further evaluate the performance of the proposed DT-enabled vehicular communication channel model. Meanwhile, we intend to further

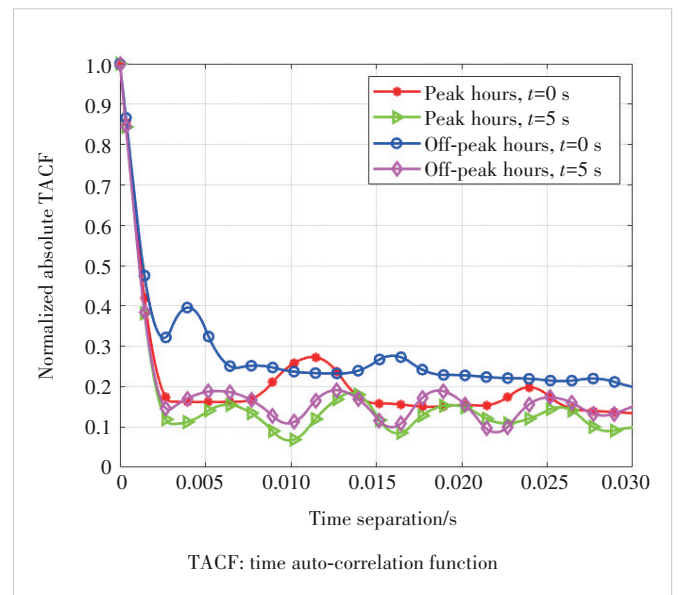


Figure 9. TACFs with varying time instants during peak and off-peak hours

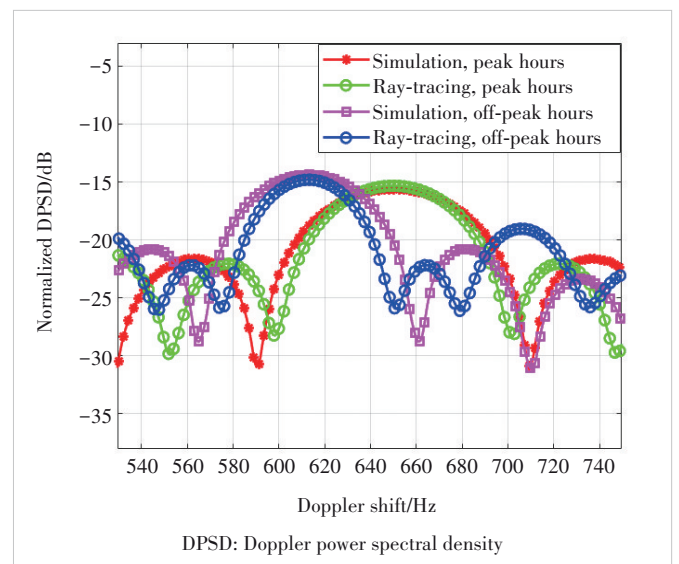


Figure 10. Comparison of simulated DPSDs and RT-based DPSDs during peak and off-peak hours

validate the effectiveness and universality of the proposed DT-based channel model with real-world measurements. Specifically, we aim to collect synchronized multi-modal sensing data and channel data in dense urban scenarios, e.g., Beijing CBD. This will enable us to refine the proposed model under real-world dynamic conditions and increase its real-world deployment value.

5 Conclusions

This paper introduces a novel DT-enabled channel model for vehicular communications in Beijing CBD. The proposed model effectively integrates LiDAR point clouds, RGB images, and channel data to enhance the precision of channel modeling in complex urban environments. A reliable DT space for the Beijing CBD area has been constructed, which has provided a high-fidelity virtual environment for simulating vehicular communication channels. The developed model captures the dynamic characteristics of scatterers during peak and off-peak hours in consideration of their number, distance, angle, power, and velocity. Key channel statistical properties (TF-CF and DPSD) have been derived and simulated during different transportation periods. Simulation results show that the proposed model accurately captures channel non-stationarity and consistency, closely aligning with RT-based experimental data. Therefore, the potential of DT technology for improving vehicular communication channel modeling in urban environments is demonstrated, which can provide a reliable foundation for the design of ITSs and advanced vehicular networks.

References

- [1] CHENG X, DUAN D L, GAO S J, et al. Integrated sensing and communications (ISAC) for vehicular communication networks (VCN) [J]. *IEEE internet of things journal*, 2022, 9(23): 23441 - 23451. DOI: 10.1109/JIOT.2022.3191386
- [2] LIN X Q, KUNDU L, DICK C, et al. 6G digital twin networks: from theory to practice [J]. *IEEE communications magazine*, 2023, 61(11): 72 - 78. DOI: 10.1109/MCOM.001.2200830
- [3] ALKHATEEB A, JIANG S F, CHARAN G. Real-time digital twins: vision and research directions for 6G and beyond [J]. *IEEE communications magazine*, 2023, 61(11): 128 - 134. DOI: 10.1109/MCOM.001.2200866
- [4] HE D P, GUAN K, YAN D, et al. Physics and AI-based digital twin of multi-spectrum propagation characteristics for communication and sensing in 6G and beyond [J]. *IEEE journal on selected areas in communications*, 2023, 41(11): 3461 - 3473. DOI: 10.1109/JSAC.2023.3310108
- [5] JIANG S F, ALKHATEEB A. Digital twin aided massive MIMO: CSI compression and feedback [C]//Proc. IEEE International Conference on Communications (ICC). IEEE, 2024: 3586 - 3591. DOI: 10.1109/icc51166.2024.10622316
- [6] XIE W L, QI F, LIU L, et al. Radar imaging based UAV digital twin for wireless channel modeling in mobile networks [J]. *IEEE journal on selected areas in communications*, 2023, 41(11): 3702 - 3710. DOI: 10.1109/JSAC.2023.3310085
- [7] DING C, HO I W. Digital-twin-enabled city-model-aware deep learning for dynamic channel estimation in urban vehicular environments [J]. *IEEE transactions on green communications and networking*, 2022, 6(3): 1604 - 1612. DOI: 10.1109/TGCN.2022.3173414
- [8] ALOBAIDY H A H, JIT SINGH M, BEHJATI M, et al. Wireless transmissions, propagation and channel modelling for IoT technologies: applications and challenges [J]. *IEEE access*, 2022, 10: 24095 - 24131. DOI: 10.1109/access.2022.3151967
- [9] CHEN Y, LI Y B, HAN C, et al. Channel measurement and ray-tracing-statistical hybrid modeling for low-terahertz indoor communications [J]. *IEEE transactions on wireless communications*, 2021, 20(12): 8163 - 8176. DOI: 10.1109/TWC.2021.3090781
- [10] ZHANG Y X, HE R S, AI B, et al. Generative adversarial networks based digital twin channel modeling for intelligent communication networks [J]. *China communications*, 2023, 20(8): 32 - 43
- [11] YU Z H, LV X Z, RUI H, et al. Digital twin channel: a data-driven continuous trajectory modeling [C]//Proc. IEEE 1st International Conference on Digital Twins and Parallel Intelligence (DTPPI). IEEE, 2021: 302 - 305. DOI: 10.1109/dtpi52967.2021.9540134
- [12] REMCOM. Wireless InSite [EB/OL]. (2017-01-01)[2024-02-01]. <https://www.remcom.com/wireless-insite-em-propagation-software>
- [13] SHAH S, DEY D, LOVETT C, et al. AirSim: high-fidelity visual and physical simulation for autonomous vehicles [M]//Field and service robotics. Cham, Switzerland: Springer International Publishing, 2017: 621 - 635. DOI: 10.1007/978-3-319-67361-5_40
- [14] SCHUBERT E, SANDER J, ESTER M, et al. DBSCAN revisited, revisited: why and how you should (still) use DBSCAN [J]. *ACM transactions on database systems*, 2017, 42(3): 1 - 21. DOI: 10.1145/3068335
- [15] GUTIERREZ C A, PATZOLD M, DAHECH W, et al. A non-WSSUS mobile-to-mobile channel model assuming velocity variations of the mobile stations [C]//Proc. IEEE Wireless Communications and Networking Conference (WCNC). IEEE, 2017: 1 - 6. DOI: 10.1109/WCNC.2017.7925795
- [16] JAECKEL S, RASCHKOWSKI L, WU S B, et al. An explicit ground reflection model for mm-wave channels [C]//Proc. IEEE Wireless Communications and Networking Conference Workshops (WCNCW). IEEE, 2017: 1 - 5. DOI: 10.1109/WCNCW.2017.7919093
- [17] BAI L, HUANG Z W, DU H H, et al. A 3-D nonstationary wideband V2V GBSM with UPAs for massive MIMO wireless communication systems [J]. *IEEE Internet of Things journal*, 2021, 8(24): 17622 - 17638. DOI: 10.1109/JIOT.2021.3081816
- [18] International Telecommunication Union. Guidelines for evaluation of radio interface technologies for IMT-2020, preliminary draft new report ITU-R M, document R15-WP5D-170613-TD-0332 [R]. 2017
- [19] HANEDA K, NGUYEN S L H, KARTTUNEN A. Measurement results and final mmMAGIC channel models, Rep. H2020-ICT-671650-mmMAGIC/D2.2 [R]. 2017
- [20] BAI L, HUANG Z W, LI Y R, et al. A 3D cluster-based channel model for 5G and beyond vehicle-to-vehicle massive MIMO channels [J]. *IEEE transactions on vehicular technology*, 2021, 70(9): 8401 - 8414. DOI: 10.1109/TVT.2021.3100389
- [21] KYOSTI P, MEINILA J, HENTILA L, et al. WINNER II channel models, version 1.1 [R]. 2007.
- [22] MARTÍNEZ À O, EGGERS P, DE CARVALHO E. Geometry-based stochastic channel models for 5G: extending key features for massive MIMO [C]//Proc. IEEE 27th Annual International Symposium on Personal, Indoor, and Mobile Radio Communications (PIMRC). IEEE, 2016: 1 - 6. DOI: 10.1109/PIMRC.2016.7794648
- [23] PÄTZOLD M. *Mobile radio channels* [M]. 2nd ed. Chichester, UK: Wiley, 2012
- [24] WANG C-X, LV Z, CHEN Y, et al. A complete study of space-time-frequency statistical properties of the 6G pervasive channel model [J]. *IEEE transactions on communications*, 2023, 71(12): 7273 - 7287. DOI: 10.1109/TCOMM.2023.3307144

Biographies

LU Mengyuan received her BS degree in engineering from the School of Software, Shandong University, China in 2024. She is currently pursuing her master's degree at the same institution. Her research interests focus on AI-based 6G vehicular communications.

BAI Lu (lubai@sdu.edu.cn) received her PhD degree in information and communication engineering from Shandong University, China in 2019. From 2017 to 2019, she was a visiting PhD student with Heriot-Watt University, UK. From 2019 to 2022, she was a post-doctoral researcher with Beihang University, China. She is currently a professor with Shandong University. Her general research interests are in areas of wireless communications and artificial intelligence, subject on which she has published more than 50 journal and conference papers and 2 books, held 5 patents, and participated in formulating 5 Chinese standards. She has received IEEE VR Best Paper Award, Science and Technology Progress Award of China Transport and Logistics Association, and TaiShan Scholar Award. She was a recipient of the Young Elite Scientist Sponsorship Program by China Association for Science and Technology. She has served as a member of the Technical Program Committee and session chair for several international conferences. She is currently an associate editor of *IET Communications* and a member of the IEEE P1944 Standard Group.

HAN Zengrui received his BS degree in information and communication engineering from the School of Information and Communication Engineering, University of Electronic Science and Technology of China in 2024. He is currently pursuing a PhD degree at the School of Electronics, Peking University, China. His current research interest is AI-based channel modeling.

HUANG Ziwei received his BS degree in communication engineering from Chongqing University, China in 2019 and PhD degree from the School of Electronics, Peking University, China. His current research interests include wireless communication channel measurements and modeling, including vehicular channel measurements and modeling, UAV channel modeling, and AI-based channel modeling. He was a co-recipient of IET Communications Best Paper Award: Premium Award.

LU Shiliang is pursuing his master's degree at the School of Software, Shandong University, China. His research interest focuses on MIMO channel modeling.

CHENG Xiang received his joint PhD degree from Heriot-Watt University and The University of Edinburgh, UK in 2009. He is currently a Boya Distinguished Professor with Peking University, China. His research interests include channel modeling, wireless communications, and data analytics, the subjects on which he has published more than 280 journal articles and conference papers, nine books, and held 26 patents. He was a recipient of the IEEE Asia-Pacific Outstanding Young Researcher Award in 2015 and the Xplorer Prize in 2023. He is a subject editor of the *IET Communications* and an associate editor of the *IEEE Transactions on Wireless Communications*, *IEEE Transactions on Intelligent Transportation Systems*, and *IEEE Wireless Communications Letter*. He has been a highly cited Chinese researcher since 2020. In 2021 and 2023, he was selected into two world scientist lists: the World's Top 2% Scientists released by Stanford University and the top computer science scientists released by Guide2Research.